1. Dominik GNAŚ[1], 2. Michał STYŁA[1], 3. Przemysław ADAMKIEWICZ[12], 4. Wiktoria ZAWADZKA

Research and Development Center of Information Technologies (CBRTI) (1), University of Economics and Innovation in Lublin (2)
ORCID: 1. 0000-0002-8169-9700; 2. 0000-0002-1141-0887; 3. 0000-0003-3425-9566. 4. 0009-0008-8139-1555

doi:10.15199/48.2024.04.49

In-building object tracking and tracing using ultra-wideband technology and temporal distance scaling methods

Abstract. *This thesis describes the implementation of the author's ultra-wideband (UWB) marker system in terms of its use in large-scale warehousing, asset management and as an in-building navigation system. The work encompasses both the hardware solution and the software and algorithmic part.*

Streszczenie. *Niniejsza praca opisuje implementację autorskiego 4systemu znaczników ultra-szerokopasmowych (UWB) w ujęciu zastosowania w magazynach wielkopowierzchniowych, przy zarządzaniu środkami trwałymi oraz jako system nawigacji wewnątrzbudynkowej. Praca obejmuje sobą zarówno rozwiązania sprzętowe jak i część programową oraz algorytmiczną (**Śledzenie i namierzanie obiektów w budynku przy użyciu technologii ultraszerokopasmowej i metod czasowego skalowania odległości**).*

Keywords: Ultra-wideband technology, Radiolocation, Asset management systems, In-building navigation system
Słowa kluczowe: Technologia ultraszerokopasmowa, Radio-lokalizacja, Systemy zarządzania środkami trwałymi, System nawigacji wewnątrzbudynkowej

Wstęp

In-building location solutions are increasingly sought after in service and warehouse buildings, as well as in public institutions for the rapid localisation of assets and people [1-5]. Ultra-wideband technology offers fast localisation in two- and three-dimensional space with high precision [6-9]. The appropriate selection of numerical algorithms allows for the visualization of the solution [10-20].

This paper presents the hardware solution and computational algorithms for an ultra-wideband (UWB)-based building localisation system. The embedded software solution how the tag and anchor control algorithm works, is also presented. The measurement results, accuracy, data transmission method, and how the measurement uncertainty is calculated will also be presented.

Hardware solution

In the hardware solution, two devices can be distinguished, namely the marker and the anchor. Both devices use 6.5 GHz (the third channel of the high band) for communication. The marker is a battery-powered device whose position is determined by the system. The marker is equipped with environmental sensors such as temperature and humidity and pressure and temperature sensors. In order to reduce the tag's energy consumption as much as possible, it is equipped with an accelerometer to wake the device from deep sleep mode.

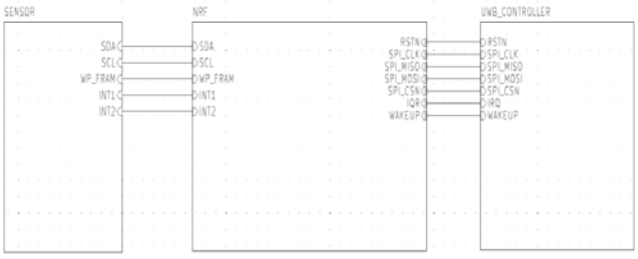

Fig. 1. General wiring diagram of the UWB marker

Figure 1 shows the general wiring diagram of the device. The central part is the nRF52832 microcontroller, which manages the device. The SPI bus is used to communicate with the DWM1000(UWB) module, while the sensors are connected using the I2C bus. Figure 2 shows the PCB mosaic. When placing the components on the board, attention had to be paid to the lengths of the paths and the ability of some components to influence others. The PCB's top (red) and bottom (green) layers are shown. Based on the mosaic, a board was made on FR4 laminate.

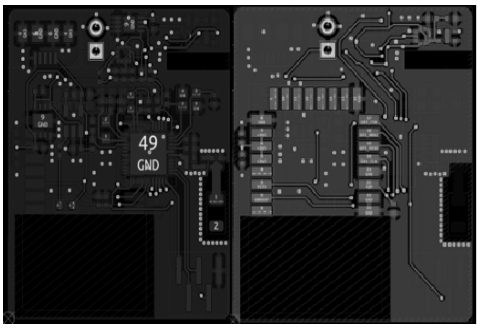

Fig. 2. PCB mosaic top layer (red) and bottom layer (green)

Figure 3 shows the finished soldered PCB with components. The soldering process was done automatically with limited human intervention.

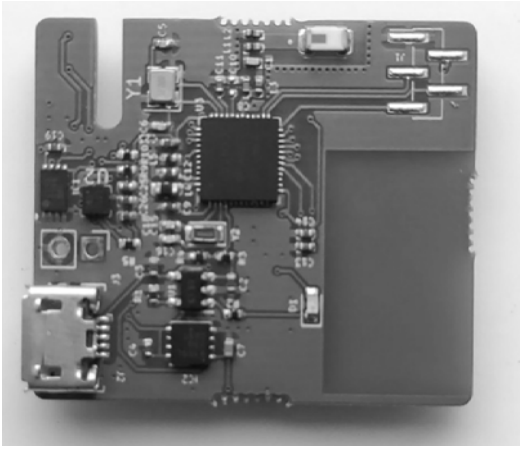

Fig. 3. The actual marker layout

The anchor module is more complicated as it had to be able to communicate with an external server via the

internet. In order to save on the number of cables, the PoE (Power over Ethernet) standard was used for the power supply, which enables data and power devices to be transmitted via a single twisted pair cable. The following is a simplified electrical diagram of the anchor.

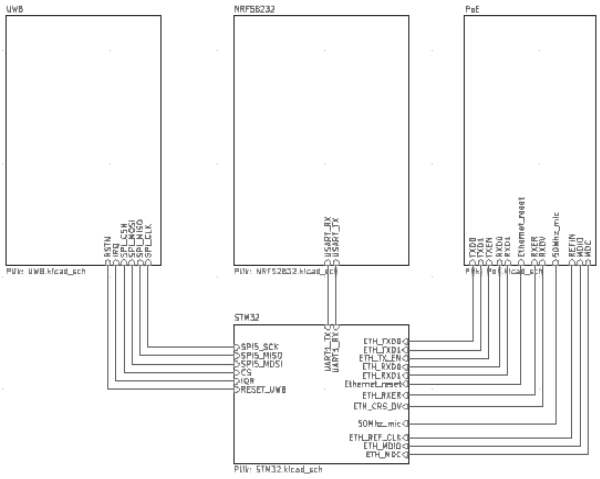

Fig. 4. Simplified electrical diagram of the anchor

Correctly making the connections in the anchor was very important due to the use of an Ethernet connection. The paths associated with the symmetrical signals should have the same impedance, which requires them to be made in such a way that they have the same length. Therefore, microwaves were used to adjust the path impedance.

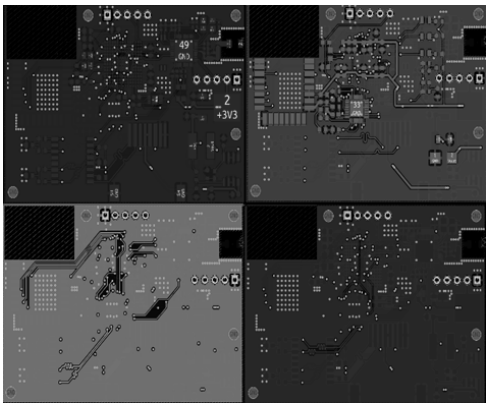

Fig. 5. PCB mosaic top layer (red) bottom layer (green) first layer inside (yellow) second layer inside (violet)

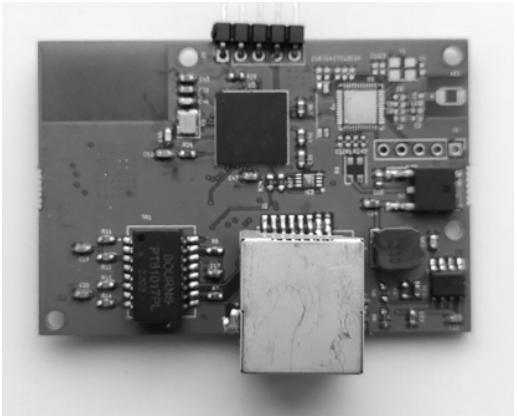

Fig. 6. The actual anchor module layout

Embedded software

The embedded software is an integral part of the system as it manages the operation of the measurement devices. Writing optimised embedded software allows the devices to work quickly. It is also possible to define device rules. Figure 7 shows the anchor and marker algorithm. The embedded system's operating algorithm works as follows. The marker is the device that initialises the distance measurement. The measurement starts by including the marker by an external interrupt from the accelerometer or environmental sensors.

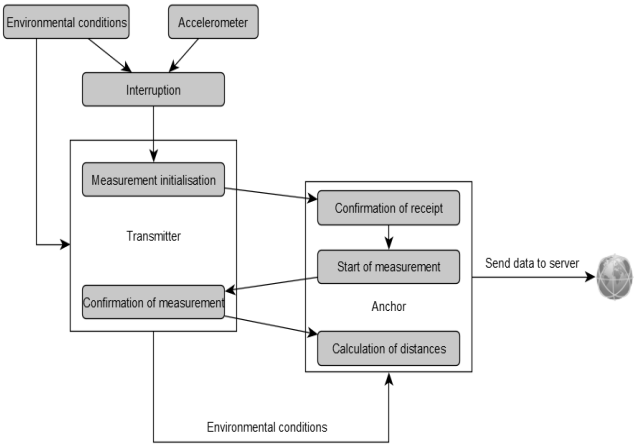

Fig. 7. Algorithm of system operation on the embedded software side

A distance measurement is taken once the marker has communicated with the anchor. The marker, together with the transmission of the time stamp, transmits the parameters of the environmental conditions. After calculating the distance between the marker and the anchor, the anchor sends the data to an external server using an Ethernet connection.

Algorithms

A time of flight (ToF) method was used to measure the distance, which is characterized by high accuracy and low measurement uncertainty. The operation of this method is based on determining the time of flight of a frame between the transmitting and receiving devices. Knowing the time of transmission and the speed at which radio waves travel (speed of light), it is possible to determine the distance accurately. This method allows multiple objects to be tracked simultaneously and makes it possible to locate them with an accuracy of several tens of centimeters. Figure 8 shows how the in-building location system under development works.

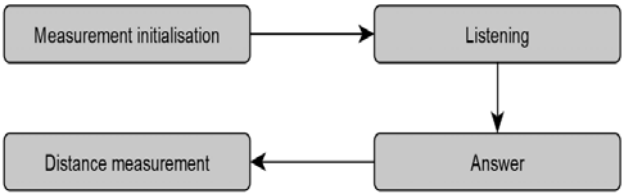

Fig. 8. Method of measuring distance by measuring the response time

The following formula shows how to calculate the distance between the anchor and the transmitter:

(1) $$tof = \frac{(t_1 - t_2)(1 - clk)}{2}$$

(2) $$d = t_{of} \cdot c \cdot 100$$

where: t1 - initialisation time, t2 - data reception time, clk - clock offset, tof – time of fly, c - speed of light.

Results

The results of the research and development work on the measurement accuracy and performance of the embedded system implemented in the tags and anchors are presented below. The following figure shows the displacement of the marker relative to the anchor, the slight variations in distance at measurement numbers 25 to 40 are due to the marker antenna being covered by the hand. This is because the electromagnetic wave velocity in air differs significantly from that in liquids.

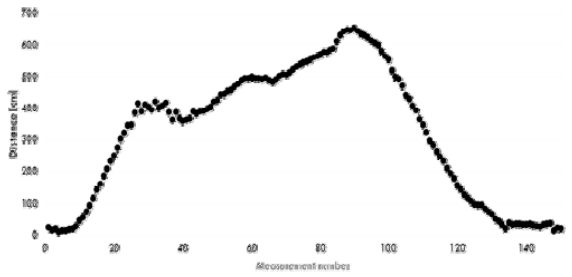

Fig. 9. Measuring distances with this system

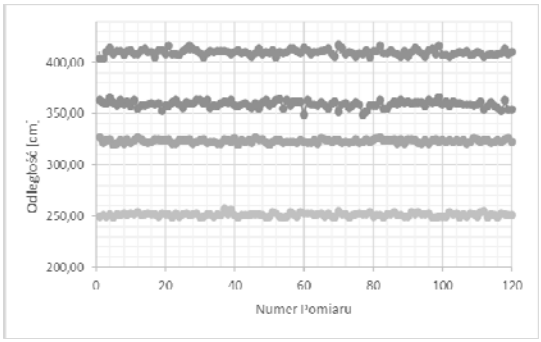

Fig. 10. Measuring the stability of the measurement system

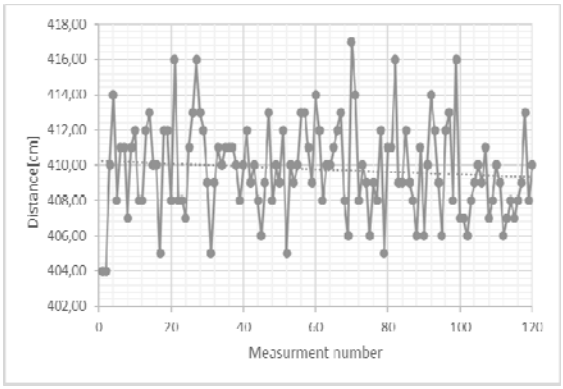

Fig. 11. Measurement error chart

Figure 10 shows the measurement of signal stability for 4 anchors simultaneously. The measurement was performed as follows: a marker was placed at one fixed location, and then the distance between this marker and the four anchors was measured.

The measurement error seen in Figure 11 can be eliminated by averaging the values and discarding outliers. The error values were measured with the marker statically aligned to the anchor, i.e. the marker was at the same distance from the anchor. The distance between the two was measured using a laser rangefinder. The measured distance between the marker and the anchor was 410.2 cm. The average standard deviation was calculated using the formula below and was 3.1. Improving accuracy and speed mainly involves changes to the embedded software. On the other hand, improvements in energy efficiency largely depend on the hardware and software layers, i.e., putting the device to sleep when it is not moving and waking it up when it moves.

(3) $$\sigma = \frac{\sqrt{\sum_{i-n}^{n}(x_i - \bar{x})^2}}{n-1}$$

where: xi - consecutive values of a given random variable in a sample, $\bar{x}$ - arithmetic mean of the sample, n - number of elements in the sample.

***Authors**: mgr inż. Dominik Gnaś, Centrum Badawczo-Rozwojowe Technologii Informatycznych Sp. z o.o. (CBRTI), ul. Rejtana 23, 35-326 Rzeszów, E-mail: dominik.gnas@cbrti.pl; mgr inż. Michał Styła, Centrum Badawczo-Rozwojowe Technologii Informatycznych Sp. z o.o. (CBRTI), ul. Rejtana 23, 35-326 Rzeszów, E-mail: michal.styla@cbrti.pl; dr Przemysław Adamkiewicz, Centrum Badawczo-Rozwojowe Technologii Informatycznych Sp. z o.o., ul. Rejtana 23, 35-326 Rzeszów, WSEI Unoversity, ul. Projektowa 4, 20-209 Lublin, E-mail: przemyslaw.adamkiewicz@cbrti.pl.*

REFERENCES

[1] Slovák J., Vašek P., Šimovec M., Melicher M. and Šišmišová D., RTLS tracking of material flow in order to reveal weak spots in production process, 2019 22nd International Conference on Process Control (PC19), (2019_, 234-238, doi: 10.1109/PC.2019.8815220.

[2] Fernandes J. R., Wentzloff D., Recent advances in IR-UWB transceivers: An overview, Proceedings of 2010 IEEE International Symposium on Circuits and Systems, (2010), 3284-3287, doi: 10.1109/ISCAS.2010.5537916.

[3] Sardar S. and Mishra A. K., UWB based dielectric material characterization using hardware/software co-design based ANN, 2013 IEEE International Conference on Industrial Technology (ICIT), Cape Town, South Africa, (2013), 1196-1200, doi: 10.1109/ICIT.2013.6505843.

[4] Thotahewa K. M. S., Redoute J. -M. and Yuce M. R., Hardware implementation of an IR-UWB coordinator node for WBAN applications, 2014 IEEE 25th Annual International Symposium on Personal, Indoor, and Mobile Radio Communication (PIMRC), Washington, DC, USA, (2014), 2168-2172, doi: 10.1109/PIMRC.2014.7136532..

[5] Zhai C., Zou Z. and Zheng L., Software defined radio IR-UWB positioning platform for RFID and WSN application, IEEE International Conference on Ultra-Wideband, Syracuse, NY, USA, (2012), 501-505, doi: 10.1109/ICUWB.2012.6340400.

[6] Fischer G., Klymenko O., Martynenko D., and Luediger H., An Impulse radio UWB transceiver with high-precision TOA measurement unit, in International Conference on Indoor Positioning and Indoor Navigation (IPIN '10)

[7] Garbaruk M., Time and frequency analysis of signals used in pulsed antenna ultra-wideband radiocommunication systems, 6th International Conference on Antenna Theory and Techniques, (2017), 276-277.

[8] Kang M., Kang J., Lee S. W., Park Y., Kim K., NLOS mitigation for low-cost IR-UWB RTLS IEEE International Conference on Ultra-Wideband (ICUWB), (2011), 96-100, doi: 10.1109/ICUWB.2011.6058931.

[9] Kolakowski J., Application of ultra-fast comparator for UWB pulse time of arrival measurement, in IEEE International Conference on Ultra-Wideband (ICUWB '11), (2011).

[10] Kłosowski G., Rymarczyk T., Niderla K., Rzemieniak M., Dmowski A., Maj M., Comparison of Machine Learning Methods for Image Reconstruction Using the LSTM Classifier in Industrial Electrical Tomography, Energies 2021, 14 (2021), No. 21, 7269.
[11] Rymarczyk T., Kłosowski G., Hoła A., Sikora J., Tchórzewski P., Skowron Ł., Optimising the Use of Machine Learning Algorithms in Electrical Tomography of Building Walls: Pixel Oriented Ensemble Approach, Measurement, 188 (2022), 110581.
[12] Kania, W., Wajman, R., Ckript: a new scripting language for web applications, Informatyka, Automatyka, Pomiary W Gospodarce I Ochronie Środowiska, 12(2022), No. 2, 4-9.
[13] Styła, M., Adamkiewicz, P., Hybrid navigation system for indoor use. Informatyka, Automatyka, Pomiary W Gospodarce I Ochronie Środowiska, 12 (2022), No. 1, 10-14.
[14] Sikora R., Markiewicz P., Korzeniewska E., Using identification method to modelling short term luminous flux depreciation of LED luminaire to reducing electricity consumption, Scientific Reportst, 13 (2023), No. 1, 673.
[15] Lebioda, M., Korzeniewska, E., The Influence of Buffer Layer Type on the Electrical Properties of Metallic Layers Deposited on Composite Textile Substrates in the PVD Process, Materials, 16 (2023), No. 13, 4856.
[16] Rymarczyk T., Kozłowski E., Kłosowski G., Electrical impedance tomography in 3D flood embankments testing – elastic net approach, Transactions of the Institute of Measurement and Control, 42 (2020), No. 4, 680-690.
[17] Kłosowski G., Rymarczyk T., Kania K., Świć A., Cieplak T., Maintenance of industrial reactors supported by deep learning driven ultrasound tomography, Eksploatacja i Niezawodnosc – Maintenance and Reliability; 22 (2020), No 1, 138–147.
[18] Kouloumtzios P., Rymarczyk T., Soleimani M., A triple-modality ultrasound computed tomography based on full-waveform data for industrial processes, IEEE Sensors Journal, 21 (2021), No. 18, 20896-20909.
[19] Kouloumtzios P., Aghajanian S., Rymarczyk T., Koiranen T., Soleimani M., An Ultrasound Tomography Method for Monitoring CO2 Capture Process Involving Stirring and CaCO3 Precipitation, Sensors, 21 (2021), No. 21, 6995.
[20] Kłosowski G, Rymarczyk T, Niderla K, Kulisz M, Skowron Ł, Soleimani M., Using an LSTM network to monitor industrial reactors using electrical capacitance and impedance tomography – a hybrid approach. Eksploatacja i Niezawodnosc – Maintenance and Reliability, 25 (2023), No. 1, 11.